Research Article

Enhancement of Flexural Strength Capacity of RC-Beams using LC-GFRP Plates with Effective Debonding Techniques

Kittipoom Rodsin
Center of Excellence in Structural Dynamics and Urban Management, Department of Civil and Environmental Engineering Technology, College of Industrial Technology, King Mongkut's University of Technology North Bangkok, Bangkok, Thailand

Kunanon Ngamkam, Rattapoohm Parichatprecha* and Jakrapong Pongpeng
Department of Civil Engineering, School of Engineering, King Mongkut's Institute of Technology Ladkrabang, Bangkok, Thailand

Tahir Mehmood
Department of Civil and Architectural Engineering, Sultan Qaboos University (SQU), Muscat, Oman

* Corresponding author. E-mail: rattapoohm.pa@kmitl.ac.th DOI: 10.14416/j.asep.2026.01.011
Received: 13 June 2025; Revised: 16 August 2025; Accepted: 21 November 2025; Published online: 27 January 2026

Abstract
Strengthening of reinforced concrete (RC) beams by externally bonded Carbon Fiber Reinforced Polymer (CFRP) is found to be a very effective method to increase their flexural strength capacity. However, the strengthening cost of the CFRP technique is very high and clients tend to avoid such expensive retrofitting methods. An alternative strengthening material, such as Glass Fiber Reinforced Polymer (GFRP), is a much less expensive material compared to CFRP. The GFRP strengthening method can achieve comparable strength gain and is an effective solution for strengthening RC beams. However, due to the lower strength and stiffness, a larger thickness of GFRP is required to obtain the target tensile strength. This increase in fiber thickness results in the commonly observed debonding failure of the GFRP-plated RC beams. Therefore, this study investigates the end anchoring technique by testing five beams under three-point bending. The first beam served as a controlled beam, while the second and the third beams were strengthened with one and three layers of GFRP to investigate the effect of the number of GFRP layers on debonding behavior. Anchored bolts were used to prevent debonding in the fourth specimen. The innovative W-shape inclined jacket technique was used for the last specimen. The test results revealed that the GFRP could effectively increase the beam's flexural strength. Nevertheless, when a larger number of GFRP layers was used, the debonding of GFRP occurred at an early loading stage. With the anchored bolted technique, the flexural strength of the RC beam was found to increase twice compared to the controlled specimen before failure due to the pulling off of the anchored bolts. Widespread shear cracks were observed near the failure stage. For the W-shape inclined jacket strengthening technique, the flexural strength was increased to a similar order as the anchored bolted technique, but the failure mode was due to slippage of the GFRP against the W-shape inclined jacket. Due to the use of a W-shape inclined jacket, the shear strength of the beam increased significantly. Therefore, the crack patterns near the final stage were controlled by flexure. The test results revealed that both techniques are effective methods to enhance the flexural strength of the GFRP-strengthened beam by achieving a similar magnitude of strength gain but failing in different failure mechanisms.

Keywords: Debonding, End anchoring system, External bonding, Flexural performance, Glass fiber reinforced polymer

1 Introduction

In the last few years, Glass Fiber-Reinforced Polymer (GFRP) has been frequently used in structural engineering applications to increase the flexural capacity of beams. This strengthening method for RC beams is frequently used because of GFRP's lightweight, transportation convenience, ease of installation, high strength-to-weight ratio, stiffness-to-weight ratio, high impact loads, good durability in harsh environments (thanks to the coated epoxy), excellent corrosion resistance, and fatigue resistance [1]–[7]. GFRP is also used as a structural reinforcement material in the Near-Surface Mounted (NSM) method, due to its higher adhesion efficiency and protection of the reinforcement material from environmental factors [8]–[10]. The externally bonded GFRP method allows easy installation at worksites with limited space and does not damage the original structure [11]–[15]. The externally bonded method of installing GFRP laminates is one of the most efficient solutions for improving the flexural capacity of RC beams. Moreover, GFRP lamination has been found to increase the load-carrying capacity at the first crack, yield, and ultimate stages. Previous research on strengthening RC beams with GFRP laminate reveals that although the strength increases with the number of GFRP layers, premature failure often occurs due to the debonding of GFRP laminates [13], [16]–[20].

As compared to Carbon Fiber Reinforced Polymer (CFRP), GFRP has a lower tensile strength and stiffness, but the elongation at rupture of GFRP is much higher, resulting in GFRP having a 3.5–5 times lower elastic modulus value [21]–[24]. Therefore, the beams strengthened with GFRP laminates exhibit lower strength at the ultimate stage but have a more ductile failure pattern compared to beams strengthened with the same number of CFRP layers [25], [26]. However, more GFRP layers would be required to achieve the same level of strength gain as achieved by using CFRP [17], [27]. Although GFRP demonstrates greater elongation capacity, offering higher deformability before failure, it generally exhibits lower long-term durability compared to CFRP. GFRP is vulnerable to moisture deterioration, alkaline environments, and UV radiation. In contrast, CFRP provides superior long-term durability and greater resistance to aggressive environments. This observation aligns with ACI 440.2R-17 [28] Section 9.4 and Bulletin 14 [29] Section 9, which specifies higher environmental reduction factors (C_E) for CFRP, indicating that GFRP is more adversely affected by adverse environmental exposure. Therefore, when considering both tensile capacity and environmental reduction factors (C_E) at the same level, the use of GFRP may not necessarily be more cost-effective than CFRP, based on prevailing market prices and industry data.

In 2018, Yoddumrong *et al*., [30], [31] initiated a study on the use of Low-Cost Glass Fiber Reinforced Polymer (LC-GFRP), a material primarily used in boat production for engineering applications. The LC-GFRP in their study was notably inexpensive, having a cost of less than 30 THB (0.88 USD) per square meter. Their results demonstrated that, despite not being originally intended for engineering purposes, LC-GFRP significantly improved the cylindrical strength of concrete. In the same study, LC-GFRP was also successfully applied to enhance the structural performance of low-strength reinforced concrete (RC) columns. Subsequently, Rodsin *et al*., [31] examined its potential for improving the compressive strength of low-strength confined concrete. Tensile strength tests by Rodsin *et al*., [32] showed that bidirectional LC-GFRP exhibited a tensile stress capacity of 377 MPa, considered adequate for structural reinforcement. In 2025, Parichatprecha *et al*., [33] selected LC-GFRP sheets as the strengthening material for pre-stressed electric transmission poles, considering their cost-effectiveness and sufficiently high tensile strength. In this study, GFRP sheets were implemented in practice to mitigate expected damage to pre-stressed poles under lateral loading. Furthermore, to enhance the performance of GFRP, Pramod and Basavaraja [34] found that incorporating GFRP with an epoxy matrix blended with Acrylonitrile-Butadiene-Styrene (ABS) has not only retained its inherent corrosion resistance but also significantly improved its mechanical properties. Specifically, the tensile strength and flexural strength increased by 107% and 103%, respectively, compared to reference specimens without ABS. Integrating GFRP with epoxy/ABS blends thus provides substantial structural performance gain while preserving its durability. Consequently, reinforced epoxy hybrid composites have gained increasing attention due to their superior mechanical performance [35], [36]. However, for beam-strengthening applications, the relatively low elastic modulus of LC-GFRP necessitates additional layers to achieve a higher fiber stiffness comparable to that required for such structural demands.

When applying more than one GFRP layer, the debonding of FRP layers before they reach their full tensile strength capacity has become a major issue in

strengthening RC structures. The research on debonding behavior of CFRP laminates, including premature bonding failure mechanisms, such as concrete cover separation, plate end debonding, and intermediate-crack debonding, has been investigated [28], [37]–[41]. Various end anchorage techniques to prevent CFRP delamination were recommended by researchers [42]–[47]. Among these methods, the steel plate with bolt anchoring system is particularly noteworthy due to its simplicity, availability of materials, efficient performance, and ease of installation, especially in beams with limited working space.

Pellegrino and Modena [48] studied the steel bolted plate anchorages system to enhance the load-carrying capacity of pre-stressed FRP. Their findings revealed that non-prestressed steel bolted plate anchorages significantly increased the ultimate load. However, despite this, it was found that the failure occurred due to FRP delamination, highlighting the limitations of the gripping capacity of the anchorage system. Yahiaoui *et al*., [49] introduced a bolt-end anchorage system (BEGFPC) using GFRP plates combined with through-bolts anchored from the top surface. The use of 10 mm bolts demonstrated a superior enhancement in ultimate load capacity and structural flexibility. However, fully drilling through the beam and accessing the top surface for bolt tightening may be impractical in real strengthening applications. Ababneh *et al*., [45] investigated a steel bolt–end anchoring system for reinforced concrete beams and reported that shear failure was accompanied by splitting of the concrete and the steel plate at the FRP edges. The anchorage performance was found to be influenced by both the bolt size and the embedding depth. In their tests, specimen AB-3 demonstrated that an embedding depth equivalent to 37.5% of the beam's cross-sectional depth was sufficient to modify the beam's failure mode. Furthermore, the authors suggested that applying a continuous reinforcement embedded at the beam ends could enhance shear resistance and mitigate shear-induced failure near the termination of the composite plate. Nonetheless, practical concerns were noted, including potential surface loss of the beam and increased susceptibility to corrosion due to the use of metallic components [50].

Another effective technique for preventing delamination involves using U-jackets made of FRP fabric. This method is widely regarded as one of the most effective anchoring solutions. Fu *et al*., [51] introduced U-jackets with angles of 45° and 90° to encase FRP laminates at both ends with and without the steel jacket. Testing revealed that 45° U-jackets were more effective than other configurations in mitigating delamination caused by the separation of the concrete cover. Appropriate U-jacket height was crucial for transferring tensile forces from the beam soffit above the reinforcement level, thereby reducing the risk of delamination. Similarly, Abdalla *et al*., [52] confirmed through both experimental testing and analytical predictions that 45° inclined FRP reinforcement, when installed using the Embedded Through-Section (ETS) technique, delivers superior shear strengthening efficiency, making it the most effective configuration for controlling shear cracking.

Most research on end anchorage has focused on preventing CFRP delamination, but there has been limited research on LC-GFRP. The influence of a very thick layer of GFRP has not been extensively studied. Therefore, the current research focuses on the study of anchorage systems to prevent delamination of LC-GFRP used for strengthening beams to enhance their flexural capacity. The study utilizes a unidirectional LC-GFRP plate in strengthening RC beams to improve their flexural strength. However, due to lower strength and stiffness, a larger thickness of GFRP is required to obtain the target tensile strength. This increase in fiber thickness results in the commonly observed debonding failure of the GFRP-plated RC beams. Therefore, to mitigate the debonding problem, a debonding prevention technique was introduced in this study. This study investigates end anchoring techniques by testing five beams under three-point bending. The first beam served as a controlled beam while the second and third beams were strengthened with one and three layers of LC-GFRP, respectively, to investigate the effect of the number of GFRP layers on debonding behavior. To prevent delamination, two widely used methods are explored: The first method involves the use of steel plates bonded with epoxy adhesive, in combination with a mechanical anchoring system known as the steel plates with bolted anchorage system, which uses commonly available bolts and steel plates. The second method investigates the development of a W-shaped inclined jacket anchorage applied, using GFRP fabric combined with angles of 45 and 135 degrees, which is easier to install and wrap around the beam to prevent delamination. The effectiveness of both methods on LC-GFRP strengthening is investigated in this study.

This research presents an innovative application of low-cost glass fiber-reinforced polymer (LC-GFRP), originally developed for non-structural

purposes such as boat construction, for the structural strengthening of reinforced concrete (RC) beams. The aim is to offer an alternative to the currently prevalent use of CFRP. Since LC-GFRP possesses significantly lower stiffness compared to CFRP, an increased number of LC-GFRP layers is required to achieve comparable performance. However, increasing the number of layers was found to heighten the risk of premature debonding due to the greater laminate thickness and the associated reduction in overall stiffness. Furthermore, the empirical equations for FRP strengthening design provided by ACI 440 do not explicitly recommend the use of multiple FRP layers. Therefore, to alleviate design concerns and mitigate debonding failures in thick LC-GFRP laminates, this study specifically investigates two anchorage systems: 1) a modified steel plate with bolted anchorage tailored for LC-GFRP, and 2) a recently proposed W-shape inclined jacket design with optimized fiber angles. The findings of this study demonstrate that these retrofitting strategies can significantly improve flexural performance, ductility, and strain utilization. Moreover, it addresses the critical issue of debonding in thick LC-GFRP layers (three-layer configuration), for which there is currently limited experimental data. By emphasizing cost-effectiveness and practical field application, this research contributes to the development of accessible and sustainable retrofitting solutions for vulnerable concrete structures, particularly in regions with limited resources.

2 Materials and Methods

2.1 *Material properties*

The materials used in the experimental program, including concrete, steel reinforcement, GFRP, and epoxy, were determined through laboratory testing conducted by the authors. The details and test results are presented as follows.

2.1.1 Concrete

In this study, the concrete mix ratio by weight was chosen as 1: 0.60: 2.20: 2.67 for cement: water: gravel: sand, respectively. A total of 18 standard concrete cylinders (∅ 150×300 mm) were prepared to determine the compressive strength of the concrete. All the concrete cubes were cured for 28 days and kept in a controlled lab environment before testing. The average compressive strength was found to be 26.0 MPa.

2.1.2 Steel rebar

Steel bars with a diameter of 6 mm (RB6) and 12 mm (DB12) were used for stirrups and longitudinal reinforcement, respectively. The tensile properties of the steel bars were determined by conducting the tensile test using a Universal Testing Machine (UTM). The tensile strength and elastic modulus of the 12 mm deformed rebar were found to be 592.06 MPa and 198.14 GPa, respectively, and 321.17 MPa and 196.15 GPa for 6 mm round rebar. The mechanical properties of steel reinforcement are shown in Table 1. Two steel bars (DB12) were located at the upper and lower sections of the beam as the main longitudinal reinforcement, as shown in Figure 1. The closed stirrups were used to avoid shear failure.

2.1.3 GFRP properties

A unidirectional GFRP fabric was used for the strengthening of the beam specimens. A total of six specimens were tested to observe the tensile stress and strain behavior of the GFRP used. The GFRP wrap test specimens were prepared with one and three layers, with a thickness of 0.25 mm for each layer. The GFRP coupons were prepared and tested in the INSTRON tensile test machine to obtain peak load, breaking load, displacement at peak load, displacement at breaking load, stress at peak, strain at peak, stress at 0.2% yield, strain at 0.2% yield, and Young's modulus. The failure patterns of LC-GFRP are illustrated in Figure 2, and the stress-strain relationships are presented in Figure 3. The average ultimate strength and ultimate elongation of LC-GFRP fabric were found to be 1217 MPa and 1.98%, respectively, while additional tensile tests on GFRP and CFRP fabrics reported tensile strengths of 2350 MPa and 3500 MPa, with an elastic modulus of 76.00 GPa and 200.00 GPa, respectively, as presented in Table 2.

Table 3 presents a comparative analysis of the cost per tensile capacity of three types of fiber-reinforced polymers (FRPs) employed in structural strengthening, namely CFRP, GFRP, and LC-GFRP. The evaluation begins with the consideration of the thickness and unit price of each material, followed by the calculation of the ultimate tensile capacity per one-meter width. These tensile capacities are subsequently adjusted using the environmental reduction factor in accordance with the provisions of ACI 440, in order to account for potential deterioration due to environmental effects. This adjustment reflects the

possibility that a greater quantity of GFRP may be required compared to CFRP to achieve an equivalent level of strength. Thereafter, the required width of each FRP to provide an ultimate tensile capacity of 100 kN per one-meter length is determined, and the corresponding cost per 100 kN tensile capacity is calculated. The labor cost for installation, fixed at 100 THB per square meter (based on a quotation from Thai Carbon Fiber Company Limited), is then incorporated into the analysis. Finally, the cost per tensile load of 100 kN is evaluated for each FRP type, showing that GFRP and LC-GFRP exhibit lower costs per tensile load by approximately 32% and 108%, respectively, when compared with CFRP.

2.1.4 Epoxy resin adhesive.

The beams were strengthened using LC-GFRP plates with dimensions of 150 mm in width and 1540 mm in length, and 0.25 mm thickness per layer. Before the installation of the LC-GFRP plates, the beam surfaces were thoroughly cleaned. Type 1 epoxy adhesive was selected as the bonding agent to attach the LC-GFRP plates to the concrete beams. During installations, even distribution across the LC-GFRP plates was ensured. Additionally, U-shaped GFRP strips, with dimensions of 150 mm in width and 185 mm in length, were applied at both ends of the beam to prevent the premature detachment of the main GFRP plate from the concrete. Type 2 epoxy adhesive was used for this purpose, as the installation involves wet lay-up techniques with LC-GFRP fabric, ensuring efficient application. The physical and mechanical properties of these epoxy adhesives are presented in Table 4.

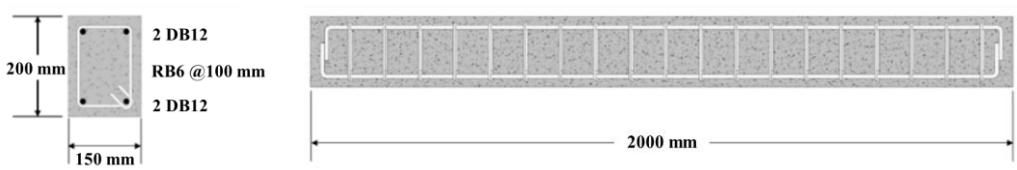

Figure 1: Section properties (a) Beam section, and (b) Side view.

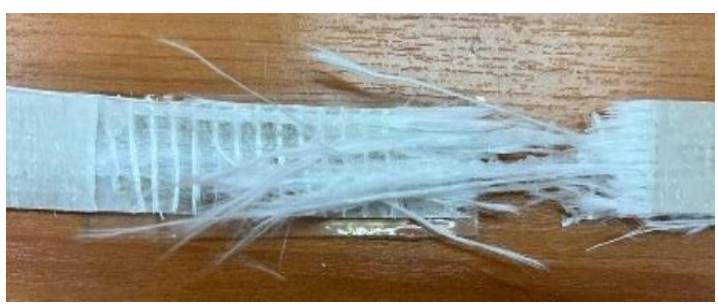

Figure 2: Failure patterns of LC-GFRP testing.

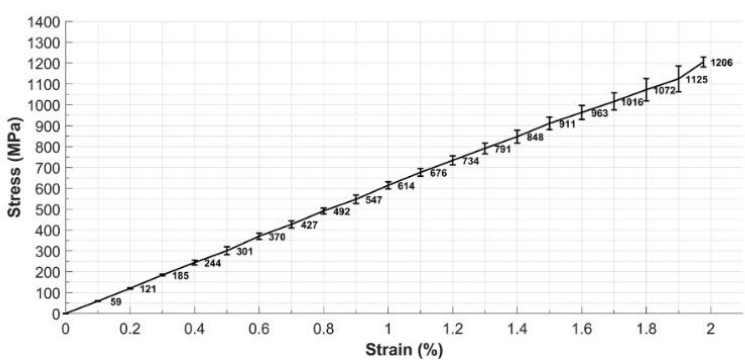

Figure 3: Typical tensile stress-strain relationship of GFRP.

Table 1: Mechanical properties of steel reinforcement.

Material	Material	Yield Strength (MPa)	Yield Strain (%)	Ultimate Strength (MPa)	Ultimate Strain (%)	Elastic Modulus (GPa)
RB6	Transverse	376.17	0.20	483.10	9.36	192.91
DB12	Longitudinal	592.06	0.30	645.18	9.38	197.35

Table 2: Average mechanical properties of FRP.

No. of GFRP Layers	Tensile Strength (MPa)	Strain at Failure (%)	Elastic Modulus (GPa)
LC-GFRP	1217.0	1.98%	61.46
GFRP	2350.0	3.10%	76.00
CFRP	3500.0	2.09%	200.00

Table 3: Comparative cost analysis of CFRP, GFRP, and LC-GFRP.

Property	CFRP	GFRP	LC-GFRP
Thickness (mm)	0.167	0.350	0.250
Unit Price (THB/m²)	780.00	450.00	29.60
Ultimate strength (kN per 1-meter width)	584.50	822.50	304.00
Environmental reduction factor, C_E	0.85	0.50	0.50
C_E-adjusted Ultimate strength (kN per 1-meter width)	497	411	152
Area required per strength 100 kN per 1-meter length (m²)	0.20	0.24	0.66
Cost per unit strength (THB/100 kN/1-meter length)	157.0	109.4	19.5
Labor cost for FRP installation (THB)	20.13	24.32	65.79
Cost per strength including labor (THB/100 kN/1-meter length)	177.12	133.74	85.26

Note: Labor cost for FRP installation was fixed at 100 THB/m² (Thai Carbon Fiber Company Limited).

Table 4: Average mechanical properties of resin adhesive.

Type	Tensile Strength (MPa)	Tensile Modulus (GPa)	Tensile Strain (%)	Density (kg/m^3)
Type 1	38.5	5.01	0.69	0.28
Type 2	52.6	6.97	0.62	0.25

2.1.5 Pull-off tests

Pull-off tests were conducted to evaluate the bond strength between the concrete substrate and both the GFRP plates and steel studs. The results are shown in Table 5. For the GFRP plate tests, as illustrated in Figure 4(a), five specimens were prepared using three-layer plates (50 × 50 mm) bonded to the beam surface with Type 1 epoxy adhesive. After curing, the testing equipment was installed using pre-installed tapered-head anchor bolts (Figure 4(b)), and additional epoxy was applied around the perimeter to ensure proper sealing and effective load transfer. Tensile loading was applied perpendicular to the bonded surface until failure occurred. In all cases, fragments of concrete remained adhered to the back of the detached GFRP plates (Figure 4(c)), indicating a substrate-related failure mechanism. The average bond strength was 3.57 MPa, with a standard deviation of 0.30 MPa. Similarly, pull-off tests were performed on five specimens with steel studs, as shown in Figure 5(a). The studs had a diameter of 12 mm, a total length of 130 mm, and an embedment depth of 80 mm, and were bonded into the concrete substrate using the same Type 1 epoxy adhesive. After curing, the testing equipment was directly attached to the studs (Figure 5(b)), and tensile loading was applied perpendicular to the bonded surface until detachment occurred (Figure 5(c)). The average bond strength was 6.96 MPa, with a standard deviation of 0.45 MPa. In both cases, these results also indicate reliable adhesive performance, as the bond strength surpassed the tensile capacity of the substrate, confirming a substrate-governed failure mechanism.

Table 5: Results of pull-off tests for GFRP plates and steel studs to concrete.

Pull-off Tests	Avg. Applied Load (kN)	Bond Strength (MPa)	Standard Deviation (MPa)
GFRP plates-concrete interface	8.92	3.57	0.30
Steel Studs –concrete	41.99	6.96	0.45

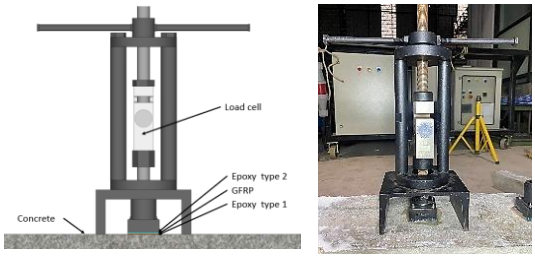

(a)

(b)

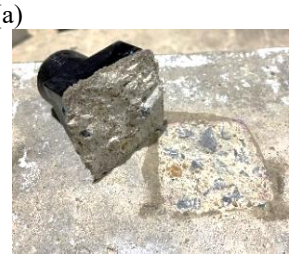

(c)

Figure 4: Pull-off test on GFRP plate (a) Pull-off testing setup, (b) Equipment installation on GFRP plate, and (c) Failure patterns.

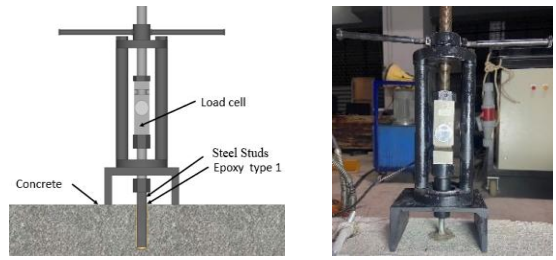

(a)

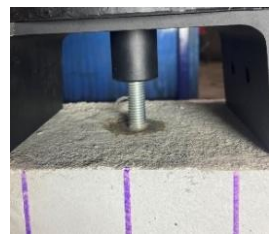

(b)

(c)

Figure 5: Pull-off test on studs (a) Pull-off testing setup, (b) Equipment installation on Studs, and (c) Failure patterns.

2.2 *Anchoring methodology*

It is important to highlight here that the selection of LC-GFRP as a retrofitting measure is mainly due to its lower cost and proven strengthening efficiency. Multiple layers of LC-GFRP were used to provide increased flexural capacity; however, multiple layers increased the tendency for debonding failure. To avoid debonding failure and ensure that LC-GFRP can be utilized to its full potential, two anchorage techniques previously proven effective for CFRP applications but still limited in research for GFRP were introduced, (a) Steel plate with bolted anchorage, chosen for its simplicity and availability in field applications, and (b) W-shape inclined jacket, selected for its ability to enhance both flexural and shear behavior while mitigating debonding through distributed confinement. These techniques will help compare the practical strengthening solutions, especially in the case of multiple LC-GFRP layers. In this research, two commonly used anchoring methods for GFRP plates were employed to compare their bonding performance, as shown in Figure 6. The first method, referred to as steel plates with bolted anchorages, utilized Mechanical Fasteners (MF). In this approach, the GFRP-strengthened beam was drilled to a depth of 80 mm (equivalent to 40% of the beam cross-sectional depth) at the plate's edge to avoid creating a weak point in the middle of the GFRP plate. Two M12 steel studs, each 130 mm in length, were embedded and secured with Type 1 epoxy adhesive. Steel plates were then positioned beneath the GFRP plate, and the entire assembly was fastened tightly to the beam using nuts and bolts, as shown in Figure 6(a). In addition to the mechanical fastening method, an alternative anchoring technique referred to as the W-shape inclined jacket was proposed. This method involves wrapping the beam with unidirectional GFRP sheets applied at inclined angles of 135° and 45° on each side, as illustrated in Figure 6(b). The same wrapping configuration was symmetrically applied to both sides of the beam to ensure effective anchorage and efficient load transfer from the GFRP plates to the beam. The W-shape jacket was bonded using Type 2 epoxy adhesive, chosen for its compatibility with the wet lay-up technique. In this process, GFRP sheets, measuring 150 mm in width (matching the soffit width) and 185 mm in height, were selected as the maximum practical dimension for field application. This height exceeds the minimum bonded length requirement of 94 mm, as calculated for a three-layer GFRP configuration in accordance with ACI 440.2R-17 [28] as given in Equation (1).

$$l_d = 0.41\sqrt{\frac{n_f E_f t_f}{\sqrt{f_c'}}} \quad (1)$$

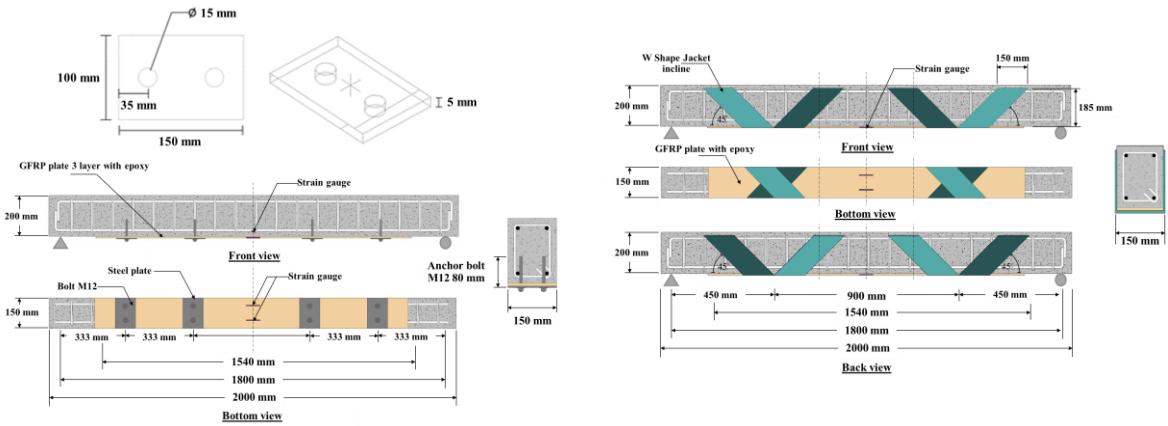

(a) (b)

Figure 6: Anchoring methods schemes. (a) Steel plates with bolted anchorages, and (b) W-Shape inclined jacket.

2.3 *Beams characteristics and test variables*

The experimental investigation comprised testing five reinforced concrete beam specimens. The cross-section of the test beams was 15 cm in width and 20 cm in height, with a total length of 2 m and an effective span of 1.8 m. Longitudinal reinforcement consisted of two DB12 steel bars positioned at both the top and bottom, while RB6 stirrups were placed at 10 cm intervals, as depicted in Figure 1. The beam specimens were prepared in various configurations. The control beam (CB) served as a reference specimen for evaluating load-carrying behavior. Two additional specimens, EB1 and EB3, were strengthened with the GFRP plate. EB1 was strengthened with a single layer of GFRP plate, whereas EB3 used a 3-layer GFRP plate. The GFRP plate used in this test was 15 cm in width and 1.54 m in length and 0.25 mm in thickness per layer. The effect of GFRP thickness on delamination behavior was investigated by comparing the debonding strain limit between EB1 and EB3. For the fourth specimen, BEB3, the performance of the steel plates with a bolted anchorages system on delamination prevention was investigated in comparison with an innovative W-shaped inclined jacket. The delamination behavior of all strengthened specimens was carefully examined, with particular focus on the effectiveness of the debonding prevention techniques. The details of all specimens are summarized in Table 6.

Table 6: Summary of specimen information.

Beams	GFRP Layer	Anchorage	Scheme
CB	-	-	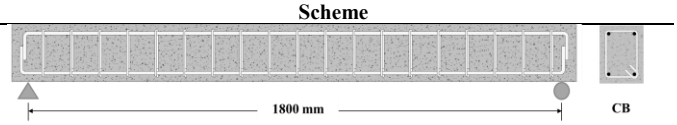
EB1	1	-	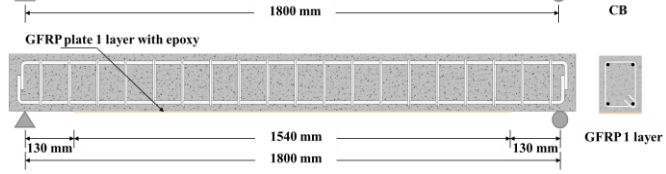
EB3	3	-	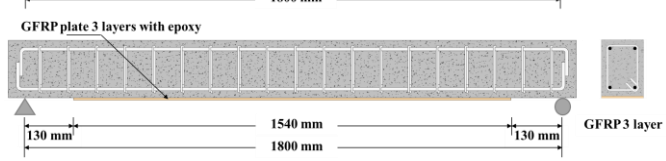

Table 6: (Continued).

Beams	GFRP Layer	Anchorage	Scheme
BEB3	3	Steel plates with bolted anchorages	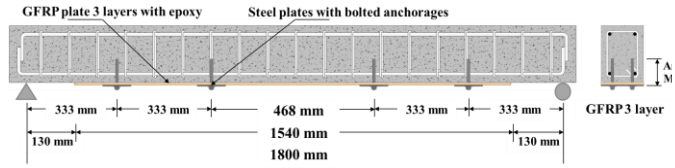
WEB3	3	W-shape inclined jacket	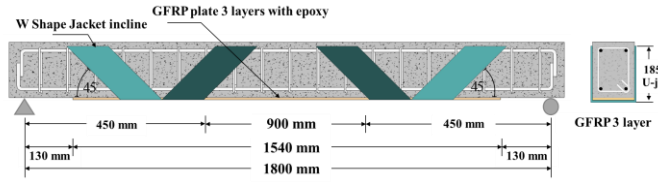

2.4 *Test setup and instrumentation*

All beams were simply supported and tested under a static three-point load. A hydraulic jack with a capacity of 500 kN was used to apply the static load to the beam specimens. The mid-span deflection was measured by installing two linear variable differential transducers (LVDTs), each with a range of 40 mm, on each beam specimen. Two strain gauges were attached to the surface of the GFRP plate, and two strain gauges were also attached to the steel bars. All sensors were connected to an automatic data logger system to record their readings continuously. During the test, a displacement-controlled scheme was applied. Crack patterns were observed, and the crack widths and spacing were measured at every 2 mm of deflection using digital photography. The test was terminated either when the applied load decreased from the maximum load or when debonding of the LC-GFRP was observed, as indicated by a sharp reduction in the strain values recorded on the GFRP surface. The failure mode was subsequently investigated. Figure 7 illustrates the arrangement of the test instrumentation and the experimental setup.

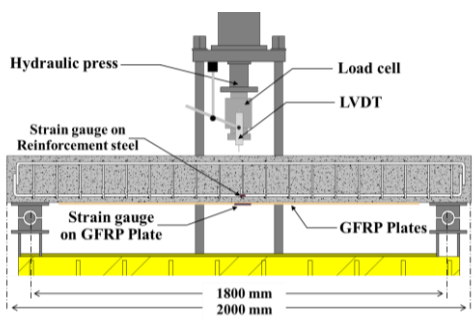

Figure 7: Placement of test instruments and loading mechanism.

2.5 *Strengthening process*

To install a GFRP plate under the reinforced concrete beam for strengthening, the surface of the concrete beam was first cleaned, and the process of sanding was performed to ensure proper adhesion of the GFRP plate. Type 1 epoxy adhesive was applied to the bottom surface of the beam. The GFRP plate was pressed against the beam to expel air bubbles, then uniformly pressed to ensure proper adhesion. The epoxy was left to cure for 24 h. Once the epoxy was cured, an anti-delamination system was installed on the BEB3 specimen to secure the GFRP plate. This process was initiated by sanding the surface of the GFRP plate and then holes of 14 mm-diameter and 70 mm deep holes were drilled. The drilled holes were cleaned with an air blower before injecting epoxy adhesive and inserting a 10 mm diameter, 10 cm long threaded steel rod into each hole. Subsequently, a steel plate with bolted anchorages was installed. This involved placing a steel plate, 100×150 mm, and 5 mm thick, to prevent stress concentration over the GFRP plate. The epoxy adhesive was applied to the steel plate before positioning it. Washers and nuts were then used to securely fasten the steel plates with bolted anchorages to the beam.

An alternative anchoring method, known as the W-Shape inclined jacket, was also employed. This method began with chamfering the corners of the concrete at the designated positions. A W-shaped inclined jacket GFRP fabric was wrapped and coated with Type 2 epoxy adhesive. The wrap was applied with one side at an inclined angle of 135 degrees and the other at 45°, as shown in Table 4. This pattern was also repeated on the opposite side of the beam. The entrapped air bubbles were removed using a roller.

The epoxy was then left to cure for 24 h to complete the installation process.

3 Results and Discussion

3.1 *Failure modes and cracking shape*

Figure 8 and Table 7 present the failure mode and the cracking pattern at the final stage of all beam specimens. The beam CB (i.e., control beam) initially exhibited vertical flexural cracks on the tension side. These cracks widened as the applied load increased. At the later stages, minor shear cracks appeared, and concrete crushing was observed in the maximum moment region of the beam specimen. Figure 8(a) shows the final cracking stage of the CB specimen.

EB1 and EB3 were the beam specimens strengthened with the GFRP plate without any anchorage systems. Both of these specimens failed in the flexural mode with GFRP debonding before reaching their rupture strains. The initial cracks were inclined and later developed into web shear cracking. Major cracks were concentrated in the maximum moment region, as presented in Figures 8b and 8c. This observation is consistent with the findings of Yahiaoui *et al*., [49], which indicate that enhanced flexural capacity without corresponding shear improvement may lead to behavior approaching a shear-governed failure mode.

The next specimen, BEB3, strengthened with GFRP and anchored using mechanical fasteners and steel plates, exhibited significantly delayed initial cracking, apparently due to the increased stiffness of the beam section. The initial cracks were similar to those observed in the previously tested specimens, i.e., vertical cracks on the tension side. However, these cracks quickly turned into inclined shear cracks, indicating that the beam behavior was controlled by shear (Figure 8(d)). As the load increased, cracks propagated through the stud regions, causing the studs to become dislodged and reducing the tensile resistance. This failure mode is consistent with the findings of Ababneh *et al*., [45], who reported that shear cracking through stud regions is typical in anchorage systems subjected to high shear demand. In contrast, the last specimen, WEB3, exhibited flexural cracking throughout the test. Minor diagonal cracks were formed as the beam approached its maximum load, indicating that the beam's behavior was controlled by flexure. The W-shaped inclined jacket GFRP wrapping effectively mitigated shear-induced failure, as illustrated in Figure 8(e). This improvement is consistent with Azevedo *et al*., [53], who reported that 45° inclined FRP reinforcement enhances shear resistance. Although anchorage configuration delays premature debonding, further considerations remain necessary when applied to GFRP strengthening systems. The GFRP possesses a significantly higher rupture strain (~2.81%) [2] compared to that of CFRP (~1.65%). The larger rupture strain increases the likelihood of interfacial slip or partial debonding before fully mobilizing the laminate's tensile capacity, which corresponds with the final failure observed in Figure 9(b).

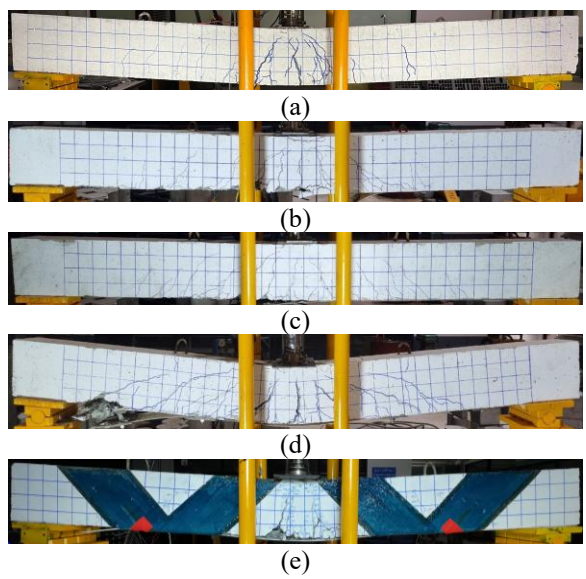

Figure 8: Failure mode of beams (a) CB, (b) EB1, (c) EB3, (d) BEB3, and (e) WEB3.

Table 7: Failure modes of beams.

Beams	Load (kN)	Displacement (mm)	Failure Mode
CB	57.7	36.0	F
EB1	81.5	30.5	F+D
EB3	97.6	17.2	F+D
BEB3	109.6	34.2	S+D
WEB3	114.9	36.8	F+D

Note: F: stands for Flexural failure; S: stands for Shear failure; D: stands for GFRP plate debonding.

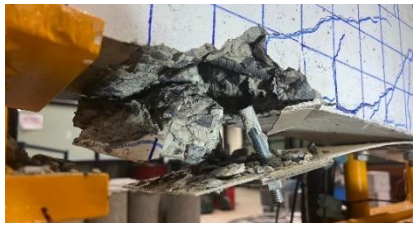

(a)

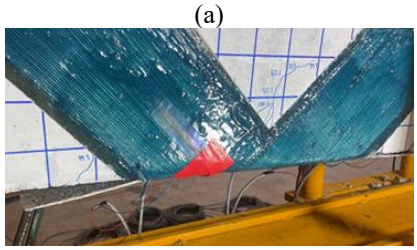

(b)

Figure 9: Close-up view of the failure modes of anchorages (a) BEB3, and (b) WEB3.

3.2 *Load-deflection response*

The load–deflection responses of the GFRP plate-strengthened beams are presented in Figure 10, while the detailed test results are summarized in Table 8. It can be observed that all strengthened beams demonstrated higher ultimate load capacities than the control beam. Moreover, the strengthened beams exhibited increased stiffness and were able to sustain load beyond the onset of debonding due to the contribution of the anchorage systems. These behavioral trends are consistent with previous findings for beams strengthened without anchorage and later enhanced with anchorage systems, as reported by Assad *et al.*, [54], confirming that the observed behavior of the tested beams is valid and consistent with established structural performance trends. For the control beam (CB), the yield load and ultimate load were recorded as 52.27 kN and 57.66 kN, while the corresponding yield and ultimate deflection were 6.13 mm and 37.97 mm. In the case of beams strengthened with GFRP, the yield load and ultimate load of EB1 (single layer of GFRP, no anchorage) increased by 31% and 42%, respectively. For EB3 (three layers of GFRP without anchorage), these values increased by 57% and 69%, respectively, compared to the control beam. Nonetheless, both EB1 and EB3 exhibited debonding of GFRP at one end, although a noticeable improvement in ductility was observed. The yield deflection increased by 25% in EB1 and 37% in EB3. Furthermore, the ductility of EB3 was lower than that of EB1 due to the higher number of GFRP layers, which caused lower strain at debonding, in accordance with the prediction from ACI 440.2R-17 [37]. These findings are consistent with the observations reported by Kaliyappan *et al.*, [26], who noted that the absence of anchorage systems limits the efficiency of multilayer GFRP strengthening because increasing the GFRP layers to match the performance of CFRP tends to accelerate premature debonding.

For beams strengthened with three layers of GFRP and anchorage systems, two configurations were tested: BEB3 (three layers with the steel plates with bolted) and WEB3 (three layers with a W-shaped inclined jacket), the test results indicated that the yield load and yield deflection of BEB3 increased by 43% and 22%, respectively, while those of WEB3 increased by 55% and 48%, respectively, compared to the control beam. At yielding, when GFRP debonding had not yet occurred, the anchorage system had little influence on the post-yield behavior, and the structural response was comparable to that of specimens without anchorage, as shown in Figure 10. Specifically, for EB3, BEB3, and WEB3, all specimens exhibited similar behavior up to the yielding. However, after yielding, the EB3 specimen experienced premature debonding and was unable to sustain additional load, whereas the BEB3 and WEB3 specimens, equipped with anchorage systems, were able to maintain load-carrying capacity and continue post-yield behavior consistently, even after GFRP debonding occurred. Subsequently, the ultimate load of BEB3 increased by 90% while that of WEB3 increased by 99% compared to the control beam. This is because the inclined anchorage system reduced shear-induced cracking, resulting in WEB3 exhibiting higher ductility compared to BEB3. In summary, when an anchorage system is provided, GFRP-strengthened beams are capable of achieving a flexural capacity comparable to those strengthened with CFRP. The present study demonstrated that the proposed GFRP strengthening configuration resulted in a 99% increase in flexural capacity, which exceeds the CFRP strength improvements reported in previous studies, including 56% by Fu *et al.* [51], 89% by Maha Assad *et al.*, [54] and 52% by Abdalla *et al.* [52]. These results confirm that GFRP, when effectively anchored, represents a highly efficient and viable alternative. Moreover, as highlighted by Rabby *et al*. [25], GFRP-strengthened beams may exhibit superior ductility at the final failure stage compared to CFRP-strengthened beams when both materials are utilized with equivalent tensile strength capacity.

Table 8: Details of test results.

Beams	GFRP layers	Anchoring System	$\triangle_y$ (mm)	$\triangle_u$ mm)	P_y (kN)	P_u (kN)	M_y (kN.m)	M_u (kN.m)	Failure Mode
CB	-	-	6.13	52.27	37.97	57.66	23.52	25.95	F
EB1	1	-	7.69	30.48	68.32	81.53	30.75	36.69	F+D
EB3	3	-	8.40	17.25	82.24	97.60	37.01	43.92	F+D
BEB3	3	Steel plates with bolted	7.45	34.17	74.88	109.64	33.69	49.34	S+D
WEB3	3	W-shape inclined jacket	9.08	36.76	80.87	114.94	36.39	51.72	F+D

Note: $\triangle_y$: yielding deflection; $\triangle_u$: ultimate deflection; P_y : yielding load; P_u: ultimate load; M_y: yielding moment capacity; M_u : ultimate moment capacity; F: Flexural failure; S: Shear failure; D: GFRP plate debonding.

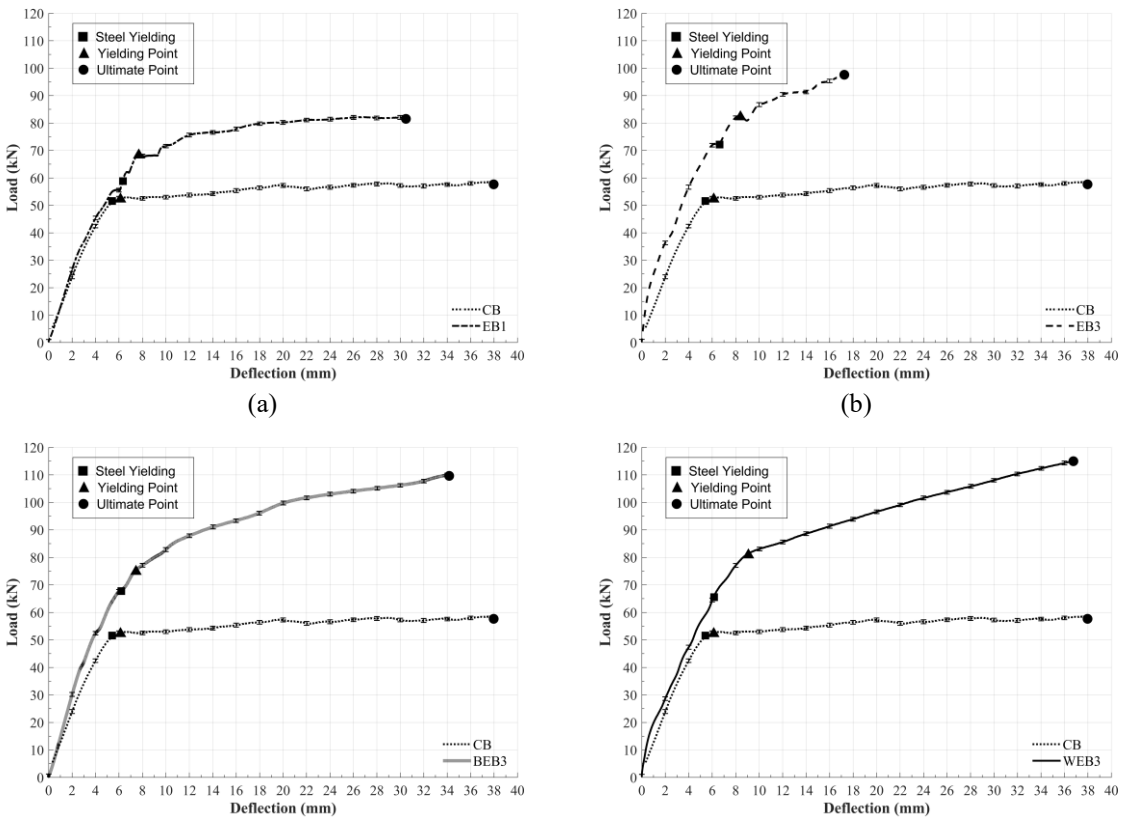

Figure 10: Comparison of load-deflection curves of all composite beams with control beam (a) EB1, (b) EB3, (c) BEB3, and (d) WEB3.

3.3 *Load-deflection response*

Figure 11 shows the average strain in the reinforcing steel, indicating that the strain in the reinforcing steel for all tested beams exceeded 0.30% at the yield point. This confirms that the GFRP-strengthened beams exhibited a ductile response, allowing continued load resistance beyond the steel yield point [47]. This corresponds to the behavior of the beams and was consistent with the results of the steel tests. Beam EB1 exhibited higher strain compared to other beams due to large cracks concentrated in the midspan region, resulting in higher localized strain and ultimately impacting the load-carrying capacity of the beam. Figure 12 illustrates the average strain in the GFRP of beam EB1. The maximum strain in the GFRP plate for EB1 was approximately 1.45%, which corresponded to 73% of the rupture strain of the GFRP. This indicates that in practical applications, additional anchorage systems may not be necessary, as the

strengthening material can be utilized to nearly its full capacity. However, for beam EB3, the maximum strain in the GFRP plate was approximately 0.97%, representing only 51% of the rupture strain of the GFRP. This demonstrates that while structural strengthening with GFRP plates can enhance the strength of the beam, because the modulus of elasticity of GFRP is about five times lower than that of steel, which limits stress transfer during displacement. To achieve full utilization of GFRP's strength, the beam must undergo higher displacement, which can lead to premature debonding of the GFRP plate. Consequently, when using three or more layers of GFRP, an anchorage system should be incorporated to prevent debonding and maximize the effectiveness of the strengthening material. With the addition of anchorage systems, the test results revealed that beams BEB3 and WEB3 achieved maximum strains in the GFRP plates, approximately 1.26% and 1.53%, respectively, corresponding to 67% and 82% of the rupture strain of the GFRP. This significant increase in strain highlights the effectiveness of the anchorage systems. The WEB3 system induced stress levels that were close to the rupture strain, nearly causing the GFRP failure. Additionally, the WEB system's performance was particularly notable for its higher elongation capacity compared to other methods. Moreover, the W-shaped inclined jacket system not only improved shear resistance, evidenced by the more linear crack propagation, but also facilitated greater utilization of the GFRP reinforcement. The maximum GFRP strain reached 1.52%, exceeding the best strain reported by Fu *et al.*, [51] (1.45%) using 45° inclined FRP U-jackets, thereby demonstrating the superior anchorage efficiency of this system.

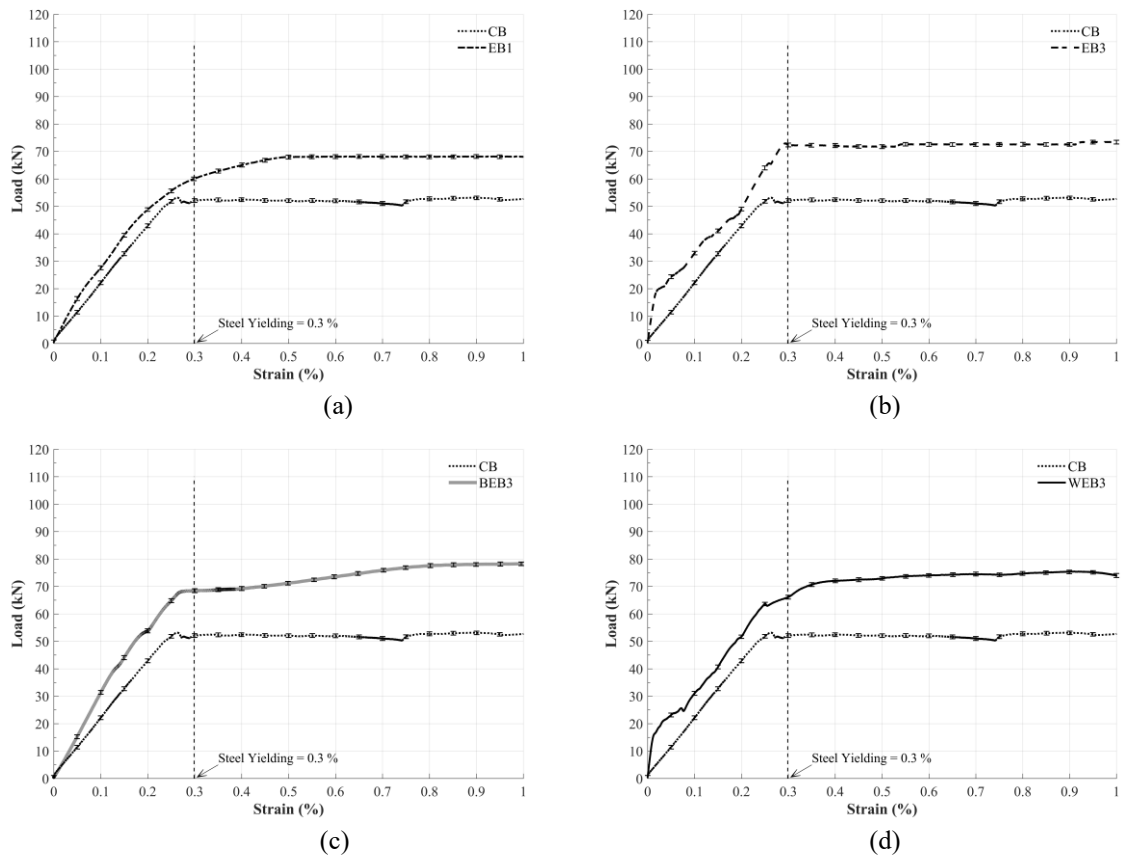

Figure 11: Comparison of load-strain at steel rebar curves of all composite beams with control beam (a) EB1, (b) EB3, (c) BEB3, and (d) WEB3.

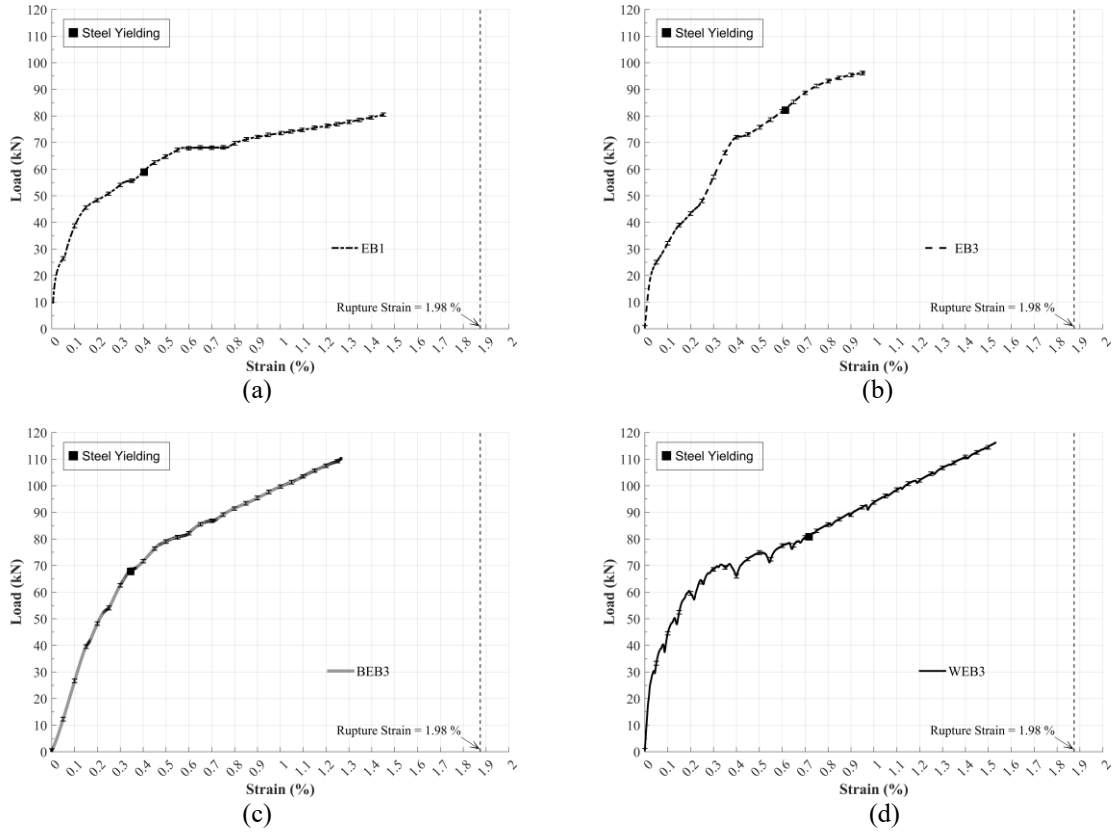

Figure 12: Comparison of load-strain at GFRP curves of all composite beams with control beam (a) EB1, (b) EB3, (c) BEB3, and (d) WEB3.

3.4 *Analytical investigations on flexural capacity of GFRP strengthened beams*

All the tested strengthened beams were analyzed using a stepwise calculation approach. The load transfer mechanism was assumed to be consistent with that of reinforced concrete (RC) beams, following the fundamental assumption that a plane section before bending remains plane after bending, as illustrated in Figure 13. This approach, which forms the basis for flexural strengthening design with FRP, is described in both ACI 440.2R-17 and fib Bulletin 14 [28], [29], which provide consistent principles for determining maximum flexural capacity. However, it should be emphasized that Bulletin 14 does not explicitly specify strain limitations for FRP that may lead to premature debonding. Consequently, to prevent premature debonding of FRP plates, the provisions of ACI 440.2R-17 were adopted for the analytical evaluation and subsequently compared with the experimental results. In this context, constraints on the strain level in the FRP plates were applied in accordance with the recommendations of ACI 440.2R-17. Furthermore, ACI 440.2R-17 specifies limiting values for the ultimate strain of the GFRP layer, as expressed in the Equations (2).

Figure 13(a) illustrates the cross-section of the beam externally reinforced with GFRP sheets, Figure 13(b) depicts the strain and internal forces within the beam, and Figure 13(c) presents the stress distribution on the surface of the test beam. The stress on the beam's cross-section can be calculated using the stress distribution method. When designing a beam externally reinforced with GFRP sheets without additional delamination prevention measures, it is crucial to consider the debonding strain of the externally bonded GFRP reinforcement (ε_{fd}) as defined in Equation (2). This strain value is used to determine the maximum allowable strain before GFRP delamination occurs. The resulting strain value establishes the operational limit for the GFRP usage in beams EB1 and EB3.

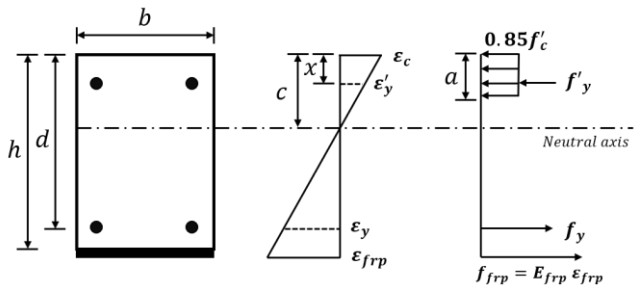

Figure 13: Stress-strain diagrams of FRP-strengthened RC beam (a) Cross Section, (b) Strain-diagram, and (c) Force Equilibrium.

$$\varepsilon_{fd} = 0.41\sqrt{\frac{f_c^{'}}{n_f E_f t_f}} \le 0.9\varepsilon_{fu} \quad (2)$$

The forces acting on the beam's cross-section can be expressed in the following form:
T_s = The tensile force in reinforcement steel given by:

$$T_s = A_s f_s \quad (3)$$

Stress in reinforcing steel (f_s) can be determined using Equations (4)–(6), with $f_s = E_s\varepsilon_s$ in the pre-yield region. For the post-yield region, the calculation of f_s was based on the approach described in the constitutive model for steel in tension shown in Figure 14, by Yalçin and Saatcioglu [55]. Experimental strain data obtained from the tests were incorporated into the model to improve the accuracy of f_s estimation in the post-yield region.

$$f_s = E_s\varepsilon_s \text{ for } \varepsilon_s \le \varepsilon_y \quad (4)$$

$$f_s = f_y + \left(\varepsilon_s - \varepsilon_y\right)\left(\frac{f_{sh} - f_y}{\varepsilon_{sh} - \varepsilon_y}\right) \quad (5)$$

for $\varepsilon_y < \varepsilon_s \le \varepsilon_y$

$$f_s = f_y + \left(f_u - f_y\right)\left[2\frac{\varepsilon_s - \varepsilon_{sh}}{\varepsilon_u - \varepsilon_{sh}} - \left(\frac{\varepsilon_s - \varepsilon_{sh}}{\varepsilon_u - \varepsilon_{sh}}\right)\right]$$

for $\varepsilon_{sh} < \varepsilon_s \le \varepsilon_u$ (6)

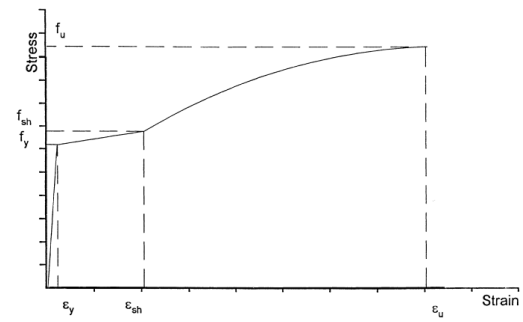

Figure 14: Stress–strain relationship for reinforcing steel in tension [49].

Tensile force in GFRP $\left(T_{frp}\right)$ can be calculated using Equations (7):

$$T_{frp} = A_{frp} f_{frp} \quad (7)$$

Where A_{frp} = area of GFRP external reinforcement (mm^2); f_{frp} = Stress in GFRP reinforcement as referenced from the strain diagram at the point where the steel reinforcement yields and the GFRP ruptures. The calculation of the compressive stress in concrete (C_c) and compressive stress in steel (C_s) can be determined using Equations (8) and (9):

$$C_c = 0.85 f_c^{'} ab \quad (8)$$

$$C_s = A_s^{'} f_y^{'} \quad (9)$$

where: A'_s, f'_y are the areas of non-prestressed steel reinforcement and compressive reinforcement, respectively.

The neutral axis depth (N.A.) can be calculated using the equilibrium equations of forces acting on the

cross-section of the tested beam, as shown in Equations (10)–(12).

$$C_s + C_c = T_s + T_{frp} \tag{10}$$

$$A_s f_y + A_{frp} f_{frp} = 0.85 f_c^{'} ab + A_s^{'} f_y^{'} \tag{11}$$

$$c = \frac{A_s f_y + A_{frp} f_{frp} - A_s^{'} f_y^{'}}{0.85 f_c^{'} \beta_1 b} \tag{12}$$

After determining the neutral axis depth for all tested beam samples, the nominal flexural strength of the section with GFRP external bonded reinforcement can be calculated using Equation (13). This calculation assumes that the bending moment at the neutral axis is equal to zero. The calculated flexural moment capacities at the yielding point and ultimate point are derived based on the strain stages identified from the strain diagram. This method adjusts the forces corresponding to different parameters to enhance the accuracy of predicting structural behavior.

$$M_n = T_{frp}(h-c) + T_s(d-c) + C_s(c-x) + C_c(c) \tag{13}$$

where M_n = the nominal flexural strength of the section with GFRP external bonded reinforcement (kN.m).

The moment–curvature diagrams of all beams obtained from the analytical model were determined using Equations (13) and (14) based on strains measured at two locations. This method, originally proposed by Kaklauskas and Ghaboussi [56], is presented in Figure 15. Compared with the control specimen, all GFRP-strengthened beams exhibited greater load-carrying capacity. For beams strengthened with single and three LC-GFRP layers without anchorage, the debonding strain specified by ACI 440 was used as the termination criterion. These beams showed clear improvement; however, in the three-layer configuration, debonding occurred soon after steel yielding, indicating that the strengthening material was not fully utilized. In contrast, beams with steel-plate (BEB3) or W-shaped inclined anchorage (WEB3) maintained their capacity after debonding and carried additional loads until LC-GFRP rupture, achieving the maximum strengthening effect. The concrete in compression and the tension steel for tension, curvature κ can be expressed as

$$\kappa = \frac{\varepsilon_t - \varepsilon_c}{h} = \frac{\varepsilon_s - \varepsilon_c}{d} \tag{14}$$

where ε_c, ε_t = denotes the strain at the extreme compression fiber of the beam; ε_s = represents the strain in the tensile reinforcement; and d = overall effective depth of the cross section.

In flexural failure, the beam undergoes ductile failure with prior warning signs. However, excessively increasing the flexural capacity through beam strengthening may result in brittle failure due to insufficient shear strength. Therefore, in the design process, it is essential to verify the shear strength capacity to ensure that the strengthened beam's capacity does not exceed the shear strength capacity, which could lead to brittle failure and pose a risk to users. The shear strength capacity can be calculated using the following Equation (15).

$$V_n = V_c + V_s \tag{15}$$

where V_n = nominal shear strength (kN); V_c = nominal shear strength provided by concrete with steel flexural reinforcement, given by:

$$V_c = 0.53\sqrt{f_c^{'}} bd \tag{16}$$

and V_s = nominal shear strength provided by steel stirrups given by:

$$V_s = \frac{A_v f_y d}{S} \tag{17}$$

In addition to determining the shear strength capacity from concrete and stirrups, the increase in shear strength of the beam due to W-Shape inclined jacket reinforcement can be calculated using Equation (18):

$$V_f = \frac{\left(A_{fv} f_{fe}\right)\left[\left(\sin\alpha + \cos\alpha\right)\right] d_{fv}}{s_f} \tag{18}$$

where V_f = nominal shear strength provided by FRP stirrups, A_{fv} represents the cross-sectional area of the U-shaped GFRP reinforcement, d_{fv} denotes are the effective depth of FRP flexural reinforcement, and s_f represents the spacing. f_{fe}= the effective stress in the FRP, is given by:

$$f_{fe} = \varepsilon_{fe} E_f \tag{19}$$

and ϵ_{fe} = effective strain in FRP reinforcement attained at failure is given by:

$$\varepsilon_{fe} = 0.004 \leq 0.75\varepsilon_{fu} \quad (20)$$

From Equations (15)–(20), the nominal shear strength of the beam (V_n) from the concrete section, and steel and FRP reinforcement is given by Equation (21):

$$V_n = V_c + V_s + V_f \quad (21)$$

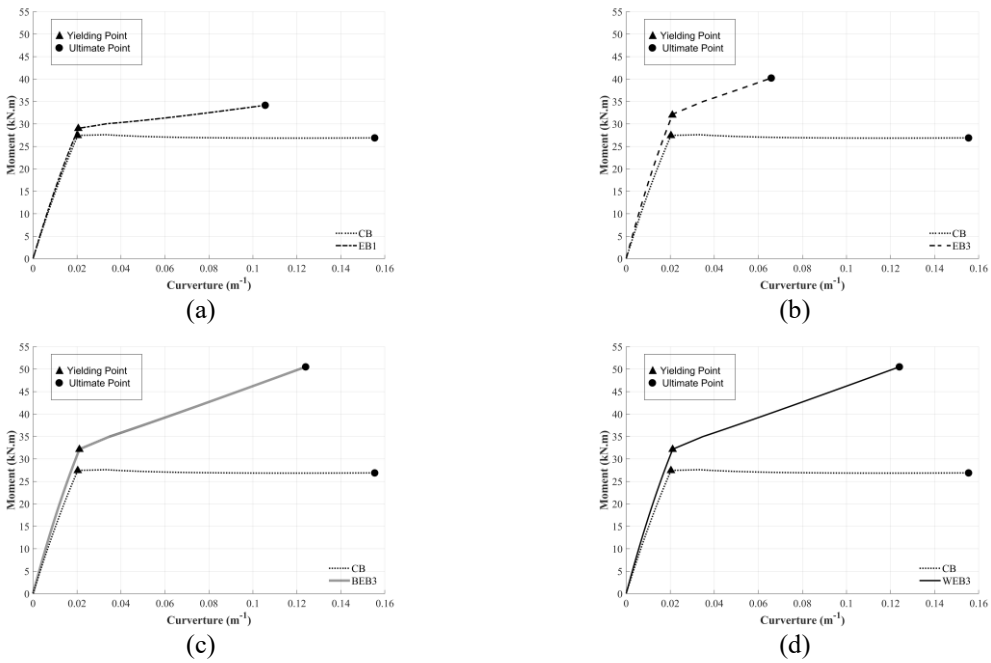

Figure 15: Comparison moment–curvature curves of all composite beams with control beam (a) EB1, (b) EB3, (c) BEB3, and (d) WEB3.

3.5 *Comparison between predictions and test results*

Table 9 summarizes the comparison between the experimental and theoretical results. It can be observed that the analytical approach employed in this study can satisfactorily predict the overall flexural behavior of the strengthened beams, showing good agreement with the experimental findings in terms of both stiffness and ultimate load capacity. However, the experimental values of the yield flexural strength for the strengthened beams were found to be slightly higher than the theoretical predictions. This discrepancy can be attributed to several interacting factors. One contributing factor is the modulus of elasticity of the composite material, which is highly sensitive to the thickness and uniformity of the adhesive layer used during bonding. Variations in the adhesive thickness can alter the strain distribution and stress transfer efficiency along the FRP–concrete interface. Furthermore, the pseudo-ductile behavior of the GFRP, which was idealized as linear-elastic in the analytical model [15], may also account for the observed difference, as the actual material response tends to exhibit gradual stiffness reduction before failure.

Nonetheless, the equations used for prediction tend to yield values lower than the experimental results, making the predictions conservative and safe for estimating the flexural strength of the strengthened beams. However, these equations should be refined to better match the experimental data [11].

To compare the remaining shear capacity of the beams, the flexural strength at the ultimate state was divided by the reduced moment capacity adjusted for safety (AV_n). When this ratio approaches to 1, it indicates an increased likelihood of shear failure. From Table 7, it was observed that beam CB exhibited a low M_n/AV_n ratio, resulting in flexural failure with visible straight cracks. While the increase in flexural

capacity due to GFRP retrofitting is acknowledged, it is important to note that the anchorage system designed to prevent premature debonding caused by stud failure led to an unintended shear failure. This occurred because the ratio of M_{eu}/AV_n also increased, approaching a value close to 1 in the BEB3 specimen. Due to this reason, the failure mode was shifted from flexural to shear. Shear failure is typically brittle and sudden, posing a significant safety concern. Although the anchorage effectively contributed to the intended enhancement of flexural capacity, this increase also resulted in a higher shear demand. The BEB3 specimen was not designed to accommodate this additional shear demand, and significant diagonal cracks due to large shear forces were observed, ultimately leading to brittle shear failure. This highlights a critical concern that increasing flexural capacity through retrofitting may unintentionally cause brittle shear failure without warning. Therefore, design guidelines must ensure that both flexural and shear capacities are thoroughly verified when retrofitting beams. When strengthened using the WEB3 system, the shear capacity of the beam increased, resulting in an M_{eu}/AV_n ratio similar to that of the control beam. Consequently, the cracks remained straight, indicating flexural failure behavior.

Additionally, from a design anchoring perspective, there are currently no clearly established or universally accepted standards specifically addressing the design of debonding-prevention or end-anchorage devices for FRP-strengthened concrete members. The experimental results of this study revealed that incorporating such devices can significantly enhance the strain level in the GFRP laminates, allowing them to reach values close to their ultimate rupture strain. This improvement enables more efficient utilization of the mechanical capacity of the composite reinforcement, thereby increasing both strength and ductility of the retrofitted beams. When compared with the analytical model predictions, the measured responses exhibited satisfactory agreement, confirming the validity and reliability of the proposed design approach. Accordingly, for the practical design of strengthening systems that include debonding-prevention devices, it is recommended to adopt the conceptual framework established in this study. The proposed system involves two efficient end-anchorage methods: 1) the use of steel plates with bolted anchorages embedded to a depth of approximately 40% of the beam section height, and 2) a W-shaped inclined jacket installed at a 45° inclination, with a width not less than that of the FRP sheet and a height maximized to the greatest practical extent. The application of these anchorage systems provides engineers with practical design guidelines for improving the overall performance, safety, and long-term reliability of GFRP-strengthened beams, while effectively mitigating premature debonding and ensuring the full development of the strengthening material's capacity.

Table 9: Comparison of flexural and shear capacity from calculation and experiment.

Beams	M_{ey} (kN.m)	M_{py} (kN.m)	$\frac{M_{ey}}{M_{py}}$	M_{eu} (kN.m)	M_{pu} (kN.m)	$\frac{M_{eu}}{M_{pu}}$	V_n(kN)	$\frac{M_{eu}}{AV_n}$
CB	23.40	23.16	1.01	25.95	26.06	1.00	73.17	0.38
EB1	26.48	24.49	1.08	36.69	33.69	1.09	73.17	0.50
EB3	32.47	27.06	1.20	43.92	38.46	1.14	73.17	0.57
BEB3	30.49	27.06	1.13	49.34	49.41	1.00	73.17	0.74
WEB3	29.50	27.06	1.09	51.72	49.41	1.05	144.61	0.38

Note: M_{ey}: experimental yielding moment capacity; M_{py}: predicted yielding moment capacity; M_{eu}: experimental ultimate Moment capacity; M_{pu}: predicted ultimate Moment capacity.

4 Conclusions

This study experimentally evaluated the flexural performance of RC beams strengthened using LC-GFRP plates with and without anti-delamination anchorage systems. The results demonstrated that a single GFRP layer can effectively enhance beam behavior and reach strain levels near the rupture limit without requiring additional anchorage. However, for three-layer configurations, premature debonding occurred shortly after yielding, preventing full utilization of the laminate capacity. Both anchorage systems investigated the steel plates with bolted anchorages and the W-shaped inclined jacket successfully delayed debonding and improved post-yield load resistance. The W-shaped system further provided notable shear enhancement, maintaining ductile behavior and enabling GFRP strain levels to reach up to 95% of the rupture strain, indicating its superior ability to improve bonding efficiency.

Analytical results from the ACI 440 model showed reasonable agreement with experimental outcomes for thin laminates but demonstrated reduced accuracy for thicker GFRP layers, suggesting that updates to current design guidelines are necessary for multilayer applications. Future work should focus on expanding the experimental database with multiple replicates to enhance statistical reliability and verify performance variability. Combining mechanical anchorage systems, such as bolt-plus-W-shape configurations, is recommended to further improve bonding efficiency and prevent slip-induced cracking. Additional research addressing durability under cyclic, fatigue, or environmental loading conditions is also essential to validate the long-term applicability of these strengthening systems for real bridge rehabilitation projects.

Acknowledgments

The authors thank King Mongkut's Institute of Technology Ladkrabang for the doctoral scholarship and laboratory facilities. The research budget was allocated by the National Science, Research and Innovative Fund (NSRF), and King Mongkut's University of Technology North Bangkok (Project no. KMUTNB-FF-68-B-41).

Author Contributions

K.R.: investigation, methodology development, reviewing and editing, funding acquisition; K.N.: experimental testing, data analysis, writing—original draft; R.P.: conceptualization, investigation, reviewing and editing, funding acquisition; J.P.: conceptualization, investigation, reviewing and editing; T.M.: conceptualization, writing—reviewing and editing. All authors have read and agreed to the published version of the manuscript.

Conflicts of Interest

The authors declare no conflict of interest.

References

[1] L. Huang, C. Zhang, L. Yan, and B. Kasal, "Flexural behavior of U-shape FRP profile-RC composite beams with inner GFRP tube confinement at concrete compression zone," *Composite Structures*, vol. 184, pp. 674–687, 2018, doi: 10.1016/j.compstruct.2017.10.029.

[2] A. Siddika, M. A. Al Mamun, R. Alyousef, and Y. H. M. Amran, "Strengthening of reinforced concrete beams by using fiber-reinforced polymer composites: A review," *Journal of Building Engineering*, vol. 25, Art. no. 100798, 2019, doi: 10.1016/j.jobe.2019.100798.

[3] S. A. Sheikh and Z. Kharal, "Replacement of steel with GFRP for sustainable reinforced concrete," *Construction and Building Materials*, vol. 160, pp. 767–774, 2018, doi: 10.1016/j.conbuildmat.2017.12.141.

[4] P. Wang, L. Ke, Z. Wang, J. Zhao, W. Li, and C. K. Y. Leung, "Effects of alkaline concentration and saline contents on degradation of tensile properties, microstructure and chemical characterization of glass fiber reinforced polymer (GFRP) rebars," *Journal of Building Engineering*, vol. 69, Art. no. 106222, 2023, doi: 10.1016/j.jobe.2023.106222.

[5] W. Ge et al., "Numerical study on flexural and bond-slip behaviours of GFRP profiled-concrete composite beams with groove shear connector," *Engineering Structures*, vol. 275, Art. no. 115226, 2023, doi: 10.1016/j.engstruct.2022.115226.

[6] P. P. Raj and A. E. Perumal, "Prediction of delamination in end milling of GFRP using ANSYS," *Australian Journal of Mechanical Engineering*, vol. 6, no. 2, pp. 39–46, 2013.

[7] K. Diharjo, A. Rakhman, W. W. Raharjo, V. Suryanti, and S. Kaleg, "Synthesis and characterization of nano active filler of pumice particle produced by sol-gel process with different precipitation temperatures for enhancing the impact properties of GFRP composite," *Applied Science and Engineering Progress*, vol. 18, no. 4, 2025, Art. no. 7750, doi: 10.14416/j.asep.2025.05.007.

[8] V. N. Nguyen and V. Van Cao, "NSM GFRP strengthening of reinforced concrete beams after exposure to fire: Experiments and theoretical model," *Journal of Composites for Construction*, vol. 27, no. 1, 2023, Art. no. 04022086, doi: 10.1061/JCCOF2.CCENG-3933.

[9] G. T. Truong, H.-H. Lee, and K.-K. Choi, "Flexural behavior of RC beams strengthened with NSM GFRP strips after exposed to high temperatures," *Engineering Structures*, vol. 173, pp. 203–215, 2018, doi: 10.1016/j.engstruct.2018.06.110.

[10] S. Ahmed, I. A. Sharaky, Y. E. Ibrahim, and A. Abdo, "Flexural response of GFRP RC beams

strengthened with side and bottom NSM GFRP bars," *Case Studies in Construction Materials*, vol. 18, 2023, Art. no. e01858, doi: 10.1016/j.cscm. 2023.e01858.

[11] I. A. Sharaky, A. S. Elamary, and Y. M. Alharthi, "Experimental and numerical investigation on the flexural performance of RC slabs strengthened with EB/NSM CFRP reinforcement and bonded reinforced HSC layers," *Engineering Structures*, vol. 289, 2023, Art. no. 116338

[12] M. H. Seleem, F. A. Megahed, A. A. M. Badawy, and I. A. Sharaky, "Performance of NSM and EB methods on the flexural capacity of the RC beams strengthened with reinforced HSC layers," *Structures*, vol. 56, 2023, Art. no. 104950, doi: 10.1016/j.istruc.2023.104950.

[13] A. N. Nayak, A. Kumari, and R. B. Swain, "Strengthening of RC beams using externally bonded fibre reinforced polymer composites," *Structures*, vol. 14, pp. 137–152, 2018, doi: 10.1016/j.istruc.2018.03.004.

[14] A. N. Nayak, A. Kumari, and R. B. Swain, "Strengthening of RC beams using externally bonded fibre reinforced polymer composites," *Structures*, vol. 14, pp. 137–152, 2018, doi: 10.1016/j.istruc.2018.03.004.

[15] B. Ramesh, S. Eswari, and T. Sundararajan, "Experimental and numerical studies on the flexural behaviour of GFRP laminated hybrid-fibre-reinforced concrete (HFRC) beams," *Innovative Infrastructure Solutions*, vol. 6, pp. 1–13, 2021, doi: 10.1007/s41062-020-00374-z.

[16] M. M. Fayyadh and H. A. Razak, "Externally bonded FRP applications in RC structures: A state-of-the-art review," *Jordan Journal of Civil Engineering*, vol. 15, no. 2, pp. 157–179, 2021.

[17] N. Attari, S. Amziane, and M. Chemrouk, "Flexural strengthening of concrete beams using CFRP, GFRP and hybrid FRP sheets," *Construction and Building Materials*, vol. 37, pp. 746–757, 2012, doi: 10.1016/j.conbuildmat. 2012.07.052.

[18] B. Ramesh, S. Eswari, and T. Sundararajan, "Flexural behaviour of glass fibre reinforced polymer (GFRP) laminated hybrid-fibre reinforced concrete beams," *SN Applied Sciences*, vol. 2, pp. 1–10, 2020, doi: 10.1007/ s42452-020-1966-2.

[19] L. Huang, B. Yan, L. Yan, Q. Xu, H. Tan, and B. Kasal, "Reinforced concrete beams strengthened with externally bonded natural flax FRP plates," Composites Part B: *Engineering*, vol. 91, pp. 569–578, 2016, doi: 10.1016/j.compositesb. 2016.02.014.

[20] N. Aravind, A. K. Samanta, J. V. Thanikal, and D. K. S. Roy, "An experimental study on the effectiveness of externally bonded corrugated GFRP laminates for flexural cracks of RC beams," *Construction and Building Materials*, vol. 136, pp. 348–360, 2017, doi: 10.1016/ j.conbuildmat.2017.01.047.

[21] M. Abolfazli et al., "Bond behaviour between CFRP, GFRP, and hybrid C-GFRP tubes and seawater sea sand concrete after exposure to elevated temperatures," *Construction and Building Materials*, vol. 392, 2023, Art. no. 131884, doi: 10.1016/j.conbuildmat.2023.131884.

[22] H. F. Hassan, M. K. Medhlom, A. S. Ahmed, and M. H. Al-Dahlaki, "Flexural performance of concrete beams reinforced by GFRP bars and strengthened by CFRP sheets," *Case Studies in Construction Materials*, vol. 13, 2020, Art. no. e00417, doi: 10.1016/j.cscm. 2020.e00417.

[23] K. Khorramian and P. Sadeghian, "Hybrid system of longitudinal CFRP laminates and GFRP wraps for strengthening of existing circular concrete columns," *Engineering Structures*, vol. 235, 2021, Art. no. 112028, doi: 10.1016/j.engstruct.2021.112028.

[24] O. Ozturkoglu, U. Yucel, C. Karademir, and E. Durmazgezer, "An experimental study on the effect of GFRP and CFRP strengthening on the static and dynamic behavior of R/C beams under progressive damage," *Applied Sciences*, vol. 14, no. 21, 2024, Art. no. 9920, doi: 10.3390/app 14219920.

[25] M. F. R. Anik, M. M. H. Asif, S. H. Raha, and S. R. Chowdhury, "A comparison between strengthened CFRP and GFRP laminated RC beam: Finite element approach," *Journal of Structural Engineering*, its Applications and Analysis, vol. 3, pp. 1–16, 2020, doi: 10.5281/ zenodo.4289927.

[26] S. P. Kaliyappan and P. Pakkirisamy, "Behavior of reinforced concrete beam with CFRP and GFRP laminates," Matéria (Rio de Janeiro), vol. 28, no. 4, 2023, Art. no. e20230222, doi: 10.1590/1517-7076-RMAT-2023-0222.

[27] P. Yoddumrong, K. Rodsin, and S. Katawaethwarag, "Experimental study on compressive behavior of low and normal strength concrete confined by low-cost glass fiber reinforced polymers (GFRP)," *in 2018 Third International Conference on Engineering*

Science and Innovative Technology (ESIT), 2018, pp. 1–4, doi: 10.1109/ESIT.2018.8665331.

[28] ACI Committee 440, Guide for the Design and Construction of Externally Bonded FRP Systems for Strengthening Concrete Structures. *American Concrete Institute*, 2017.

[29] International Federation for Structural Concrete (fib), Externally Bonded FRP Reinforcement for RC Structures (fib Bulletin No. 14). Lausanne, Switzerland: fib, 2001.

[30] P. Yoddumrong, K. Rodsin, and S. Katawaethwarag, "Seismic strengthening of low-strength RC concrete columns using low-cost glass fiber reinforced polymers (GFRPs)," *Case Studies in Construction Materials*, vol. 13, 2020, Art. no. e00383, doi: 10.1016/j.cscm. 2020.e00383.

[31] K. Rodsin, Q. Hussain, S. Suparp, and A. Nawaz, "Compressive behavior of extremely low strength concrete confined with low-cost glass FRP composites," *Case Studies in Construction Materials*, vol. 13, 2020, Art. no. e00452, doi: 10.1016/j.cscm. 2020.e00452.

[32] K. Rodsin, N. Ali, P. Joyklad, K. Chaiyasarn, A. W. Al Zand, and Q. Hussain, "Improving stress–strain behavior of waste aggregate concrete using affordable glass fiber reinforced polymer (GFRP) composites," *Sustainability*, vol. 14, no. 11, 2022, Art. no. 6611, doi: 10.3390/su14116611.

[33] R. Parichatprecha, K. Rodsin, S. Suthasupadit, T. Mehmood, and A. Nawaz, "Collapse prevention of pre-stressed electric transmission poles using glass fiber reinforced polymers," *Case Studies in Construction Materials*, vol. 22, 2025, Art. no. e04110, doi: 10.1016/j.cscm. 2025.e04110.

[34] R. Pramod and V. K. G. Basavaraja, "Investigation of the thermal and mechanical properties of glass fiber reinforced ABS/epoxy blended polymer composite," *Applied Science and Engineering Progress*, vol. 17, no. 4, 2024, Art. no. 7252, doi: 10.14416/j.asep.2024.08.003.

[35] A. D. Akinwekomi et al., "Development and characterization of hybrid particulate-fiber reinforced epoxy composites," *Applied Science and Engineering Progress*, vol. 17, no. 4, 2024, Art. no. 7391, doi: 10.14416/j.asep.2024.06.001.

[36] T. P. Sathishkumar, P. Navaneethakrishnan, and P. Maheskumar, "Thermal stability and tribological behaviors of tri-fillers reinforced epoxy hybrid composites*," Applied Science and Engineering Progress*, vol. 14, no. 4, pp. 727–737, 2021, doi: 10.14416/j.asep.2021.08.002.

[37] G. Li, T. Hu, Y. Shao, and D. Bai, "Data-driven model for predicting intermediate crack induced debonding of FRP-strengthened RC beams in flexure," *Structures*, vol. 41, pp. 1178–1189, 2022, doi: 10.1016/j.istruc.2022.05.023.

[38] T. Mohammadi, B. Wan, K. A. Harries, and M. E. Sweriduk, "Bond behavior of FRP–concrete in presence of intermediate crack debonding failure," *Journal of Composites for Construction*, vol. 21, no. 5, 2017, Art. no. 04017018, doi: 10.1061/(ASCE)CC.1943-5614.0000797.

[39] A. G. Razaqpur, R. Cameron, and A. A. B. Mostafa, "Strengthening of RC beams with externally bonded and anchored thick CFRP laminate," *Composite Structures*, vol. 233, 2020, Art. no. 111574, doi: 10.1016/j.compstruct.2019. 111574.

[40] A. Dönmez, M. Rasoolinejad, and Z. P. Bažant, "Size effect on FRP external reinforcement and retrofit of concrete structures," *Journal of Composites for Construction*, vol. 24, no. 5, 2020, Art. no. 04020056, doi: 10.1061/(ASCE) CC.1943-5614.0001070.

[41] M. A. Al-Saawani, A. K. El-Sayed, and A. I. Al-Negheimish, "Effect of shear-span/depth ratio on debonding failures of FRP-strengthened RC beams," *Journal of Building Engineering*, vol. 32, 2020, Art. no. 101771, doi: 10.1016/ j.jobe.2020.101771.

[42] C. Chen, L. Cheng, L. Sui, F. Xing, D. Li, and Y. Zhou, "Design method of end anchored FRP strengthened concrete structures," *Engineering Structures*, vol. 176, pp. 143–158, 2018, doi: 10.1016/j.engstruct.2018.08.081.

[43] D. J. Oehlers, P. Visintin, and W. Lucas, "Fundamental mechanics governing FRP-retrofitted RC beams with anchored and prestressed FRP plates," *Journal of Composites for Construction*, vol. 20, no. 6, 2016, Art. no. 04016047, doi: 10.1061/(ASCE)CC.1943-5614. 0000710.

[44] T. Skuturna and J. Valivonis, "Experimental study on the effect of anchorage systems on RC beams strengthened using FRP," *Composites Part B: Engineering*, vol. 91, pp. 283–290, 2016, doi: 10.1016/j.compositesb.2016.02.001.

[45] A. N. Ababneh, R. Z. Al-Rousan, and I. M. N. Ghaith, "Experimental study on anchoring of FRP-strengthened concrete beams," *Structures*, vol. 23, pp. 26–33, 2020, doi: 10.1016/j.istruc. 2019.09.018.

[46] Y.-F. Wu and Y. Huang, "Hybrid bonding of FRP to reinforced concrete structures," *Journal of Composites for Construction*, vol. 12, no. 3, pp. 266–273, 2008, doi: 10.1061/(ASCE)1090-0268(2008)12:3(266).

[47] K. Rodsin, A. Ejaz, Q. Hussain, and R. Parichatprecha, "Experimental and analytical studies on low-cost glass-fiber-reinforced-polymer-composite-strengthened reinforced concrete beams: A comparison with carbon/sisal fiber-reinforced polymers," *Polymers*, vol. 15, no. 19, 2023, Art. no. 4027, doi: 10.3390/polym15194027.

[48] C. Pellegrino and C. Modena, "Flexural strengthening of real-scale RC and PRC beams with end-anchored pretensioned FRP laminates," *ACI Structural Journal*, vol. 106, no. 3, pp. 319–328, 2009.

[49] D. Yahiaoui, A. Boutridd, M. Saadi, B. Mamer, and T. Bouzid, "New anchorage technique for GFRP flexural strengthening of concrete beams using bolts-end anchoring system," *International Journal of Concrete Structures and Materials*, vol. 17, no. 1, 2023, Art. no. 20, doi: 10.1186/s40069-023-00578-4.

[50] B. Fu, J. G. Teng, J. F. Chen, G. M. Chen, and Y. C. Guo, "Concrete cover separation in FRP-plated RC beams: Mitigation using FRP U-jackets," *Journal of Composites for Construction*, vol. 21, no. 2, 2017, Art. no. 04016077, doi: 10.1061/(ASCE)CC.1943-5614.0000721.

[51] B. Fu, G. M. Chen, and J. G. Teng, "Mitigation of intermediate crack debonding in FRP-plated RC beams using FRP U-jackets," *Composite Structures*, vol. 176, pp. 883–897, 2017.

[52] J. A. Abdalla, H. H. Mhanna, A. B. Ali, and R. A. Hawileh, "CFRP U-wraps and spike anchors for enhancing the flexural performance of CFRP-plated RC beams," *Polymers*, vol. 13, no. 11, 2021, Art. no. 1759, doi: 10.3390/polym13111759.

[53] A. S. Azevedo, J. P. Firmo, J. R. Correia, and J. Almeida, "Embedded through-section (ETS) technique for shear strengthening of reinforced concrete beams: Experimental and analytical study," *Engineering Structures*, vol. 333, 2025, Art. no. 120038, doi: 10.1016/j.engstruct.2022.120038.

[54] M. Assad, R. A. Hawileh, J. A. Abdalla, and T. Alkhrdaji, "Flexural behavior of CFRP-strengthened and end-anchored RC beams with large fiber anchors," *Structures*, vol. 80, 2025, Art. no. 109702, doi: 10.1016/j.istruc.2025.109702.

[55] C. Yalcin and M. Saatcioglu, "Inelastic analysis of reinforced concrete columns," *Computers & Structures*, vol. 77, no. 5, pp. 539–555, 2000, doi: 10.1016/S0045-7949(99)00228-X.

[56] G. Kaklauskas and J. Ghaboussi, "Stress–strain relations for cracked tensile concrete from RC beam tests," *Journal of Structural Engineering*, vol. 127, no. 1, pp. 64–73, 2001, doi: 10.1061/(ASCE)0733-9445(2001)127:1(64).